*MĀPAN-Journal of Metrology Society of India (September 2017) 32(3):229–241*
DOI 10.1007/s12647-017-0215-7

ORIGINAL PAPER

# Morphology, Mineralogy and Mixing of Individual Atmospheric Particles Over Kanpur (IGP): Relevance of Homogeneous Equivalent Sphere Approximation in Radiative Models

**S. K. Mishra[1]*, N. Saha[1], S. Singh[1], C. Sharma[1], M. V. S. N. Prasad[1], S. Gautam[1], A. Misra[2], A. Gaur[2], D. Bhattu[2], S. Ghosh[2], A. Dwivedi[2], R. Dalai[2], D. Paul[2], T. Gupta[2], S. N. Tripathi[2] and R. K. Kotnala[1]**

[1]CSIR-National Physical Laboratory, New Delhi, India

[2]Department of Civil Engineering, Indian Institute of Technology (IIT), Kanpur, India

Received: 17 January 2017 / Accepted: 11 April 2017 / Published online: 12 June 2017



**Abstract:** Estimation of the direct radiative forcing (DRF) by atmospheric particles is uncertain to a large extent owing to uncertainties in their morphology (shape and size), mixing states, and chemical composition. A region-specific database of the aforementioned physico-chemical properties (at individual particle level) is necessary to improve numerically-estimated optical and radiative properties. Till date, there is no detailed observation of the above mentioned properties over Kanpur in the Indo-Gangetic Plain (IGP). To fill this gap, an experiment was carried out at Kanpur (IITK; 26.52°N, 80.23°E, 142 m msl), India from April to July, 2011. Particle types broadly classified as (a) Cu-rich particles mixed with carbon and sulphur (b) dust and clays mixed with carbonaceous species (c) Fe-rich particles mixed with carbon and sulfur and (d) calcite ($CaCO_3$) particles aged with nitrate, were observed. The frequency distributions of aspect ratio (AR; indicator of extent of particle non-sphericity) of total 708 particles from April to June reveal that particles with aspect ratio range >1.2 to ≤1.4 were abundant throughout the experiment except during June when it was found to shift to high AR range, >1.4 to ≤1.6 (followed with another peak of AR i.e. >2 to ≤2.4) due to dust storm conditions enhancing the occurrence of more non-spherical particles over the sampling site. The spherical particles (and close to spherical shape; AR range, 1.0 to ≤1.2) were found to be <20% throughout the experiment with a minimum (11.5%) during June. Consideration of Homogeneous Equivalent Sphere Approximation (HESA) in the optical/radiative model over the study region is found to be irrelevant during the campaign.

**Keywords:** Morphology; Mixing-state; Mineral dust; Hematite

## 1. Introduction

Observations and modeling studies reveal that the direct radiative forcing (DRF) by atmospheric particles is uncertain to a large extent; global and annual mean RF ranges from −0.85 to +0.15 $Wm^{-2}$ [1, 2]. Mineral dust is the most uncertain component amongst the entire aerosol species in terms of net TOA (Top of Atmosphere) dust radiative effect which is reported to be −0.56 to +0.1 $Wm^{-2}$ [1]. Morphological (shape and size) analyses of atmospheric particles using Scanning Electron Microscopy (SEM) reveal that shapes of dust particles are extremely irregular [3, 4]. Morphological factors such as overall shape, sharpness of edges, and surface texture (i.e. the degree of surface roughness) affect the single scattering properties of a particle. Ignoring these morphological properties lead to uncertainties in the numerical estimation of their optical/radiative properties. Some studies [5, 6, 7] have discussed in detail about various traceability issues related to particulate measurement.

The studies based on measurement and modeling reveal that the optical properties of non-spherical particles are quite different compared to that of their volume-equivalent spheres [8, 9, 10]. Therefore, to improve the current knowledge about aerosol radiative characteristics in climate studies, and also in the retrieval of aerosol properties from ground- and satellite-based radiometric

*Corresponding author, E-mail: sumitkumarm@gmail.com

measurements, it is necessary to use the proper scattering and absorption properties of aerosols by accounting for their morphology. Many existing aerosol retrieval techniques, *e.g.*, the operational aerosol retrieval algorithm applied to the moderate resolution imaging spectroradiometer (MODIS) measurements have not incorporated the observed physico-chemical properties of particles. The effects of highly non-spherical particles with their region specific shape proportions and complex mixing states with the other chemical species cannot be ignored in the forward radiative transfer simulations [4]. Besides morphology of particles, the chemical composition of regional atmospheric particles are not well accounted for in radiative transfer simulations and remote sensing applications. Iron (in form of hematite, $Fe_2O_3$) has been observed as a major component of dust particles that influences the light absorption ability of dust [9, 11]. The regional information on proportions of particles with varying hematite content is a must for the aforesaid reasons. The effect of aspect ratio, AR on the dust scattering has been reported significant in case of dust with high hematite content [4]. Further, the estimation of optical/radiative properties of regional aerosols and retrieval of aerosol properties become extremely complex over the region where long range transported mineral dust form a heterogeneous mixture with carbonaceous species [10]. Therefore, a detailed physical and chemical characterization of particles over such regions is imperative.

The traditional characterizations of aerosols give bulk level information, not at individual particle level. The region-specific physical (size, shape and mixing state) and chemical (composition) characterization of individual particles have already been carried out over various places [4, 12–15]. Scanning electron microscopy with energy-dispersed X-ray analysis (SEM-EDX) is commonly used for single particle characterization [16, 17]. Besides morphology and composition of individual particles, mixing states of particles give the information of physical configurations in which various species are mixed together. Some of the recent studies report the individual particle characterization in Indo Gangetic Plain (IGP) at Agra and Varanasi [18–20] but no study reports the frequency distribution of AR which is extremely important parameter for accounting particle non-sphericity while simulating optical properties of aerosols.

To the best of our knowledge, there is no detailed observation of the aforementioned properties of aerosol over Kanpur in the IGP, where the existence of complex aerosols are more probable due to mixing of long-range transported mineral dust [9, 21] with the local pollutants [22, 23]. Keeping this in mind, an intensive experiment was carried out at IIT Kanpur in central IGP from April to July, 2011 to study the detailed physico-chemical properties of regional aerosols. Misra et al. [23] have provided detailed information about the experiment and the measured aerosol properties. In the present work, we discuss composition, mixing state and morphology of individual particles over Kanpur during this campaign. The classification of major particle types and the datasets generated on particle proportions with varying hematite content, and proportions of spherical and non-spherical particles over the study region have been discussed. In view of the generated database, the relevance of Homogeneous Equivalent Sphere Approximation (HESA) assumption in the optical/radiative model has been evaluated.

## 2. Sampling Site

Kanpur spreads over 260 $km^2$ area and surrounded by two main rivers, the Ganges in the North-East and the Yamuna in the south. Kanpur features a humid subtropical climate with long and very hot summers, mild and relatively short winters, dust storms and a monsoon season. Sometimes dry heat is accompanied by dust storms during intense heating in April–June. The occurrence of rain is more probable between July to September. The collection of aerosol samples for the morphological, mineralogical and mixing state analysis at individual particle level was carried out over Kanpur city (IITK; 26.52°N, 80.23°E, 142 m msl), India on weekly basis from April to July, 2011.

## 3. Theoretical Background, Experimental Details and Methodology

The morphological parameter (AR) of aerosol is calculated based on earlier research work [4, 24, 25]. The calculation of AR requires information about the maximum projection and width of the particle which are defined below:

(1) Maximum projection (or the length of the longest projected dimension): the largest separation between points on the particle convex perimeter.
(2) Width (w): the largest length of the particle perpendicular to the maximum projection.

Using the parameters (1) and (2), AR is calculated by Eq. (1)

$$AR = \frac{maximum\ projection}{width} \tag{1}$$

Note that AR of a sphere is equal to one. AR gives information on extent of particle non-sphericity and is a major input parameter for the calculation of optical properties of non-spherical particles.

Ambient atmospheric particles, particularly $PM_{2.5}$ (particles with aerodynamic diameter <2.5 μm) and $PM_{10}$ (particles with aerodynamic diameter <10 μm), were collected using $PM_{2.5}$ and $PM_{10}$ samplers at the IITK sampling site. The surface morphology and topology of individual particles together with their elemental composition were determined using a Scanning Electron Microscope (SEM: ZEISS EVO MA-10) equipped with an energy dispersive spectrometer (EDS: Oxford Link ISIS 300) at CSIR-National Physical Laboratory. The width and maximum projection of individual particles were calculated using the observed SEM micrographs and Image J software (http://rsbweb.nih.gov/ij/); see Mishra et al. [4] for more details on the adopted approach.

## 4. Result and Discussion

In this section, we present a detailed classification of observed particles based on composition, mixing state and morphology of individual particles. The SEM micrographs of collected particles reveal that most of the particles are non-spherical. The proportions of particles with varying Fe weight percentage and the monthly frequency distributions of morphological parameter (AR) of particles have also been discussed.

### 4.1. Classification and Type of Individual Atmospheric Particles

Figure 1 shows the ternary plots of aerosol composition based on spot EDS analysis. Ternary diagrams are useful for understanding the aerosol mixing state information [26–29]. Data within the triangle represent particles that are internal mixtures of the three elements shown in apices [28, 30]. Based on ternary plots, composition of atmospheric particles are broadly classified as (a) Cu-rich particles mixed with carbon and sulphur (b) dust and clays mixed with carbonaceous species (c) Fe-rich particles mixed with carbon and sulfur, and (d) Calcite (CaCO3) particles aged with Nitrate.

#### *4.1.1. Cu-Rich Particles*

The circle number 1 in Fig. 1a shows the Cu (>50%) rich particles mixed with C and S. These particles are purely of anthropogenic origin mainly from brake wear and Cu smelters etc. [31]. Few particles were observed to be a binary mixture of Cu and C. As opposed to the crustal origin, presence of C and S in the aerosols suggest anthropogenic origin (like vehicle brake wear, Cu smelters and ore processing etc.) in the locality nearby the sampling site. Schroeder et al. [32] have shown that Cu associated with fine mode particulate matter tends to originate from combustion activities whereas Cu associated with that of coarse mode particles is likely to originate from windblown soil and dust. Worldwide windblown dust has an estimated mean emission of 0.9–15 $\times$ $10^6$ kg/year of Cu into the atmosphere (WHO [33] and references therein). Based on a survey done in Western Europe, Cu has also been found to have originated from brake wear, which acts as the most dominant source in urban ambient air [31]. Cu-rich particles in the atmosphere can be very harmful to human beings due to various associated health effects like gastrointestinal effect, hepatic effect as well as lung problems, but very little study has been done on the carcinogenicity of Cu. Figure 2 shows the morphology, composition and mixing state of individual particles classified in this family. Here, we find variable Cu morphology like honey comb structures (Fig. 2a, b), plates (Fig. 2c), plates with grains (Fig. 2d) and semi-externally mixed spheres and cylinders (Fig. 2e, f). Particles were observed to be in coarse size regime.

#### *4.1.2. Dust/Clay Particles Mixed with Carbonaceous Species*

The circle number 2 in Fig. 1b shows majorly quartz particles; while circle number 3 shows aluminosilicates mixed/aged with C (refer to Fig. 3 for morphological information). The circle number 4 in Fig. 1c shows Fe-rich particle mixed with carbonaceous species while circle number 5 shows mainly carbonaceous particles. The Figs. 3 and 4 show the morphology of aforementioned particles. Figure 3 shows the morphology, composition and mixing state of individual dust/clay particles mixed with carbonaceous species based on SEM-EDS analysis. Figure 3a shows Fe-rich dust particles aged with C and N. Figure 3b shows a dust particle (with arrow) where carbon fractal seems to be adhered to the surface of the dust particle. Also, here we find some flaky structures. Figure 3c shows dust particle (with arrow) heavily aged with C. Here also, we observe some flakes. Figure 3d shows porous curved flakes majorly comprised of aluminosilicates. Figure 3e shows flakes of aluminosilicates heavily aged with C. Figure 3f shows the dust particle while Fig. 3g shows many flaky structures (generally clays) aged with C.

Complex mixing of aerosol has also been reported over other places in the world. The African dust (close to dust source and far away regions) comprises of Fe either internally mixed with silicates (clays) or existing in the form of Fe oxide grain in and at the surface of particles [34–38]. Over Africa, the urban pollution was found to be mixed with mineral dust, which could be studied using a nadir-looking high spectral resolution lidar (HSRL) onboard the German research aircraft during the Saharan

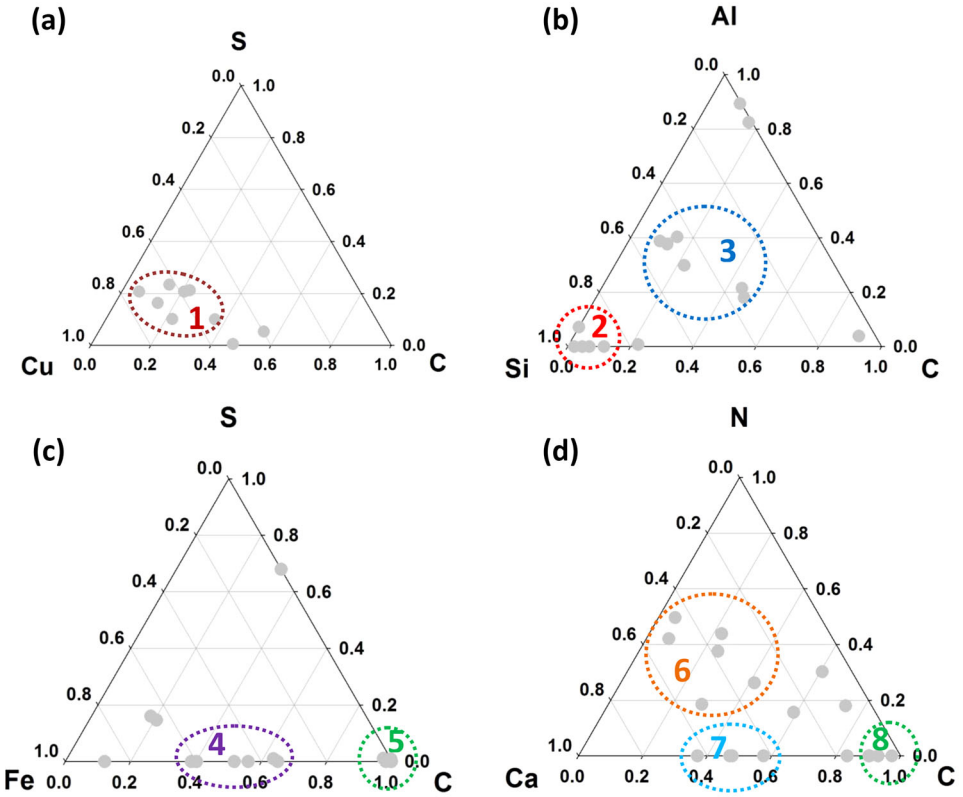


**Fig. 1** Ternary plots of aerosol composition based on SEM-EDS analysis **a** Cu rich particles mixed with carbon and sulfur **b** dust/clays mixed with carbonaceous species **c** Fe rich particles mixed with carbon and sulfur **d** Calcite ($CaCO_3$) particles aged with nitrate

Mineral Dust Experiment (SAMUM) [39]. Also, in Asia, based on microscopic techniques, Clarke et al. [40] found the mineral dust to be mixed with the pollutants emitted from industrialized areas.

### *4.1.3. Carbonaceous Particles*

Figure 4 shows the morphology, composition and mixing state of individual carbonaceous particles based on SEM analysis. We observed various carbon fractal morphologies. Note that optical properties of carbonaceous particles are extremely sensitive to their morphologies [41, 10]. A carbon fractal is a chain of carbon monomers which we defined as fresh, semi-aged, and aged, based on their morphology. Here, carbon monomer is the primary particle with a set of swirled graphitic sheets in a spherule. In general, these carbon fractals are released in the atmosphere due to anthropogenic activities (like combustion, vehicular emission). Just after emission, the fractals are generally open chain, so we referred them as fresh fractals while with varying time, these fractals have a tendency to be more compact to minimize the energy. The fractals with highly compact shapes have been referred as aged fractals while less compact are referred as semi-aged fractals. Figure 4a–d shows these fractal types with micron and coarse sizes. Here, it is important to mention that the fresh fractals are more absorbing compared to that of their volume equivalent spheres, and that the difference in this absorption enhances with increasing size (Mishra and Ramanathan; under review). Carbon morphologies shown in Fig. 4a–d are of graphitic nature while Fig. 4e shows carbon which may belong to family of organic carbon [41]. Pure carbon fractal is hydrophobic in nature but the surface of the black carbon fractal acts as active sites for adsorption of various chemical species and hence the fractal is turned in to hygroscopic aerosol. Thus, black carbon fractal can act as CCN or ice nuclei [42, 43].

### *4.1.4. Calcite Particles*

Ternary plot (Fig. 1d) reveals the phase and mixing information about the calcite ($CaCO_3$) particles. Figure 1d shows majorly (1) calcite particles aged with N (circle 6); (2) fresh calcite particles (circle 7); and (3) calcite particles heavily aged with C (circle 8). Figure 5a–c show the morphologies of nearly pure calcite ($CaCO_3$) particle, calcite particle aged/mixed with N and calcite rich mineral dust particle aged/mixed with N, respectively.

In Asia, mineral dust particles were observed to have nitrates formed due to heterogeneous reactions with nitrogen oxides [44, 45]. During a field campaign, Matsuki et al. [46] observed that at least 60–90% of the Ca rich particles form a reactive nitrogen film which contains $NO_3^-$. The uptake of the acidic gas (like NOx) and water vapor by

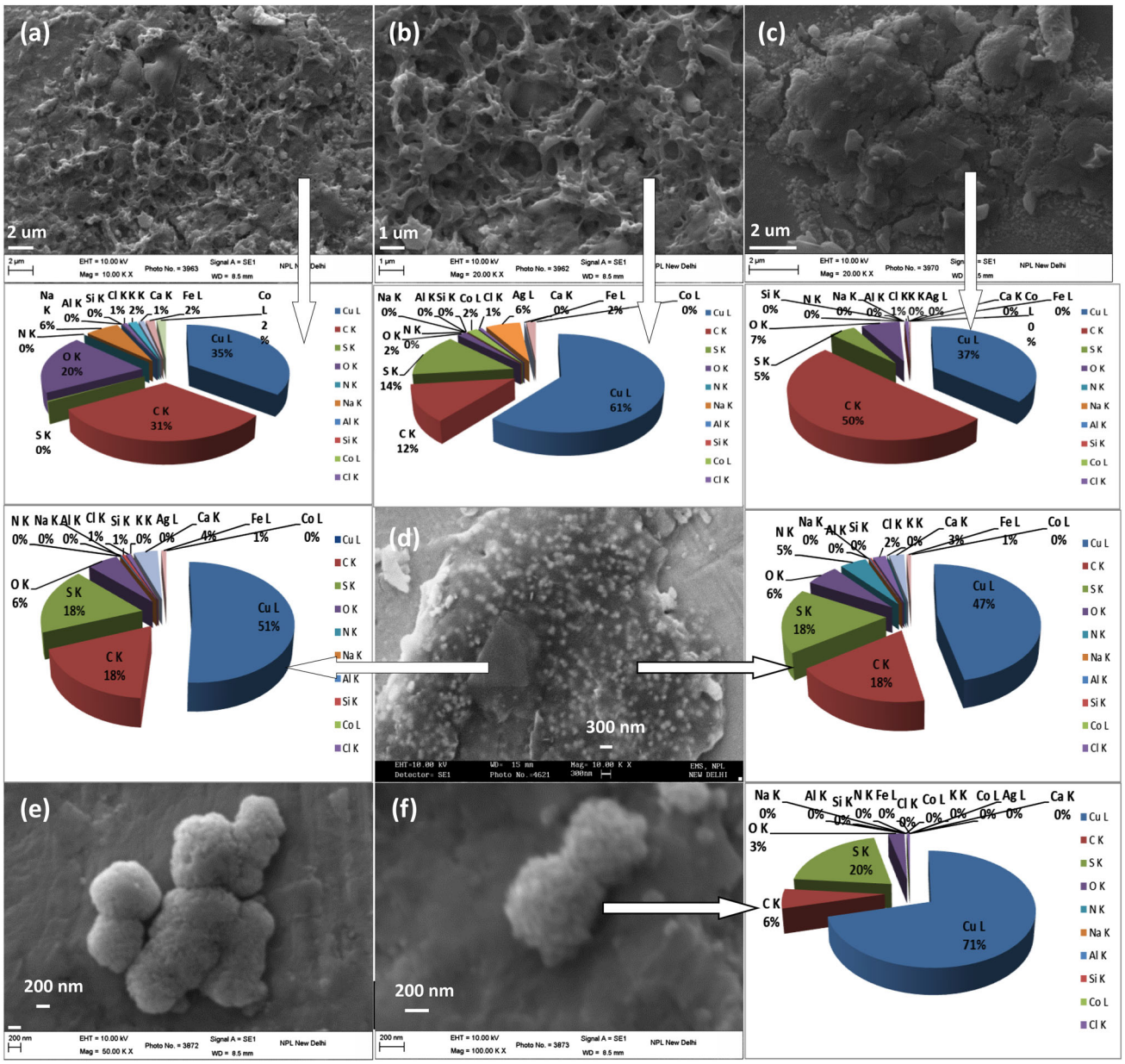


**Fig. 2** Morphology, composition, and mixing state of individual Cu rich particles based on SEM-EDS analysis

calcite particle gives rise to aging of calcite particle with N. Earlier research works show that calcite ($CaCO_3$) and dolomite ($MgCO_3{\cdot}CaCO_3$) react with $HNO_3$ gas in atmosphere to form extremely hygroscopic $Ca(NO_3)_2$ or $Mg(NO_3)_2$ species which deliquesce under sub-saturated atmospheric conditions [47–50]. Matsuki et al. [46] reported that a large numbers of Ca rich particles were of spherical shape due to uptake of $HNO_3$ gas during long range transport. However, in the present study, we found ellipsoidal Ca-rich particles. It is also known that after aging with other soluble aerosol components, the mineral dust particles are characterized with enhanced hygroscopicity, and altered sizes and shapes [47–49] with more efficient CCN [51] characteristics.

### *4.1.5. Biological Particles*

Based on the characteristic morphology and composition of the analysed particles, we identified some biological particles. The biological particles (both dead and alive) have been reported with abundance in C and O and minor amounts of Na, Mg, K, P, Si, Fe, Cl, Al and Ca [52, 53]. In general, the biological particles are broadly defined to include microorganisms, viruses, bacteria, fungal spores,

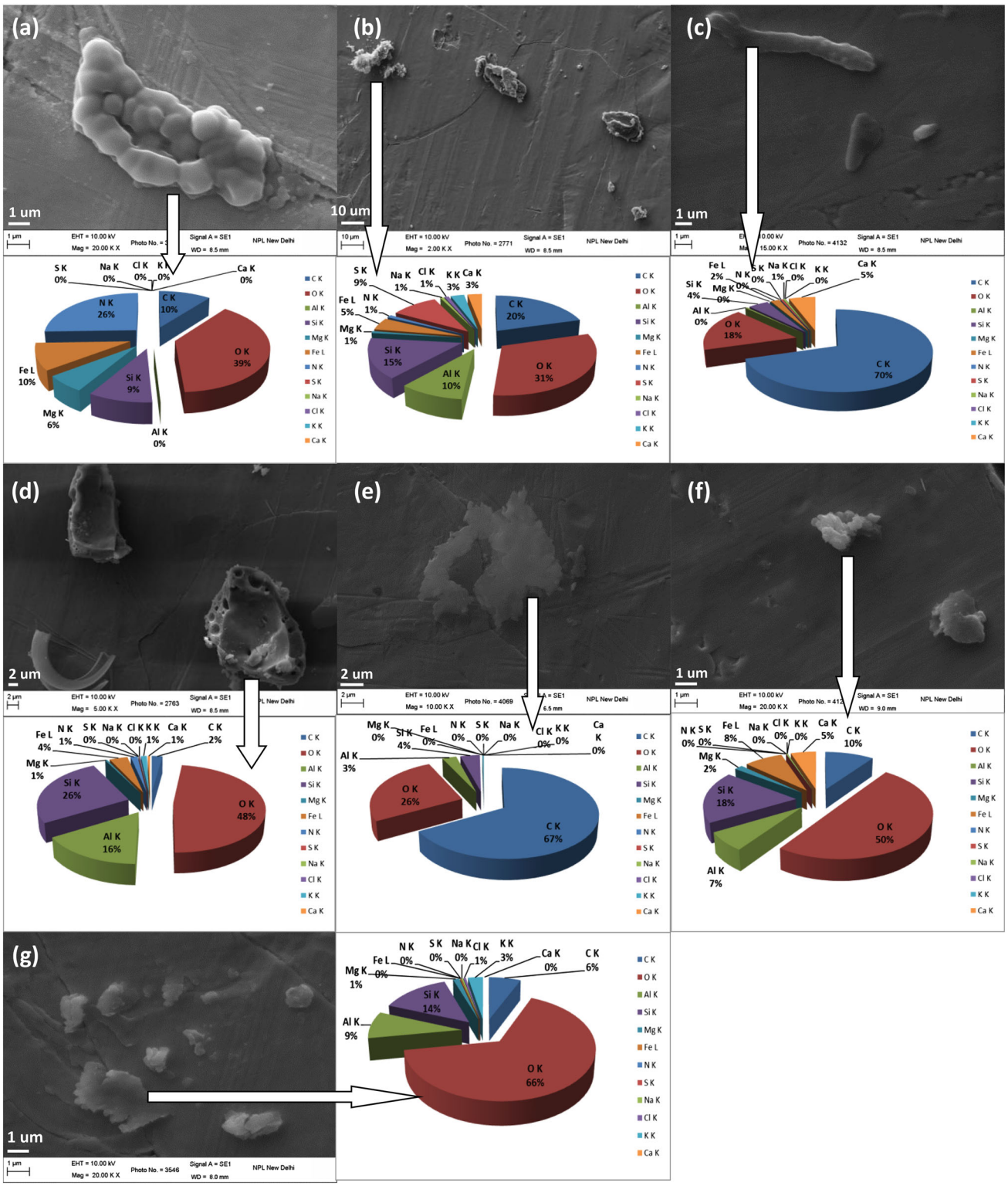


**Fig. 3** Morphology, composition, and mixing state of individual dust/clay particles mixed with carbonaceous species based on SEM-EDS analysis

pollen and plant debris etc. Occurrence of such particles in the atmosphere has been reported in many previous studies [54–56]. Figure 6 shows the morphology and composition of some individual biological particles based on SEM-EDS analysis. Particle-A is mainly rich in C and N while particle-B is rich in C. Particle-A is of spherical shape with

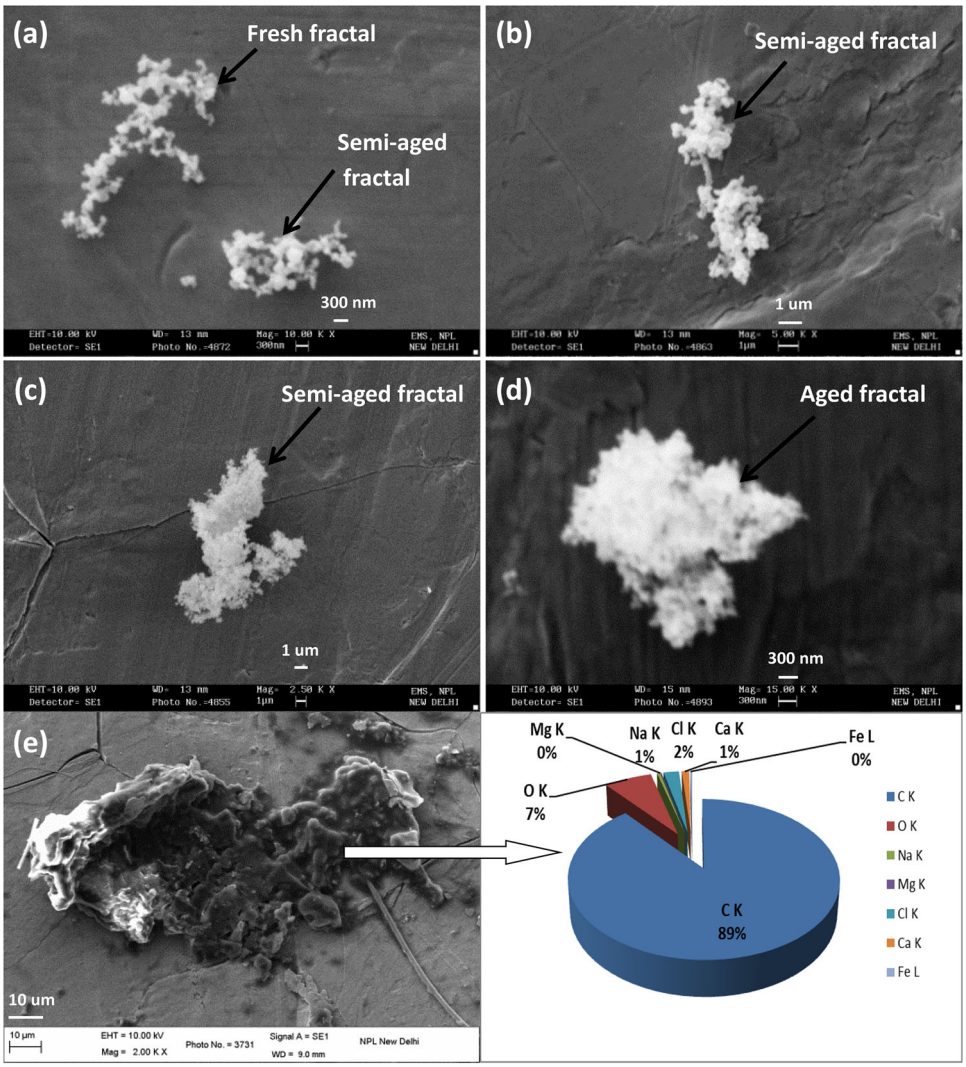


**Fig. 4** Morphology, composition, and mixing state of individual carbonaceous particles based on SEM-EDS analysis

pores in a symmetric fashion. The morphology of this particle closely resembles with that of Chenopodiaceae (Goosefoot Family) pollens (http://www.cabq.gov/airquality/todays-status/pollen/pollen-identification). The shape of the Chenopodiaceae pollen is similar to a golf ball with 15–100 pores over the pollen surface and its size ranges from 20 to 35 µm. The chenopod plants are common in the deserts and their growths are more favorable in saline or alkaline soils (http://www.desertmuseum.org/books/nhsd_chenopodiaceae.php). In India, Deotare et al. [57] found this pollen family source near the Kanod lake in Thar Desert. Presence of this pollen in Kanpur suggests likely dust transport from Thar Desert.

#### *4.1.6. Anthropogenic Particles*

Further, we also observed some other types of anthropogenic particles, whose morphology and composition are shown in Fig. 7. The SEM image of coarse range porous particles (Fig. 7a) and the high magnification image of a single particle (Fig. 7b) show the particle topography comprising of rod/needle like (∼100 nm dia) structure. The spot EDS analysis reveals that this particle is mainly composed of vanadium with traces of Cl and K, indicating combustion-related source. An increase in direct combustion of crude oil residues in power plants has been related to enhanced concentration of vanadium in air [33]. We observed micron size vanadium rich particles with rod/needle like structures which closely resemble with the morphology of experimentally synthesized vanadium oxides nanotubes (http://www.microscopy.ethz.ch/VOx-NTs.htm). The coal-fired Panki thermal power plant which is situated ∼3 km from our sampling site is the likely source of vanadium particles. Also, the combustion of the carbonaceous matrix releases vanadium along with fly ash in the atmosphere [33]. Figure 7c shows coarse-size

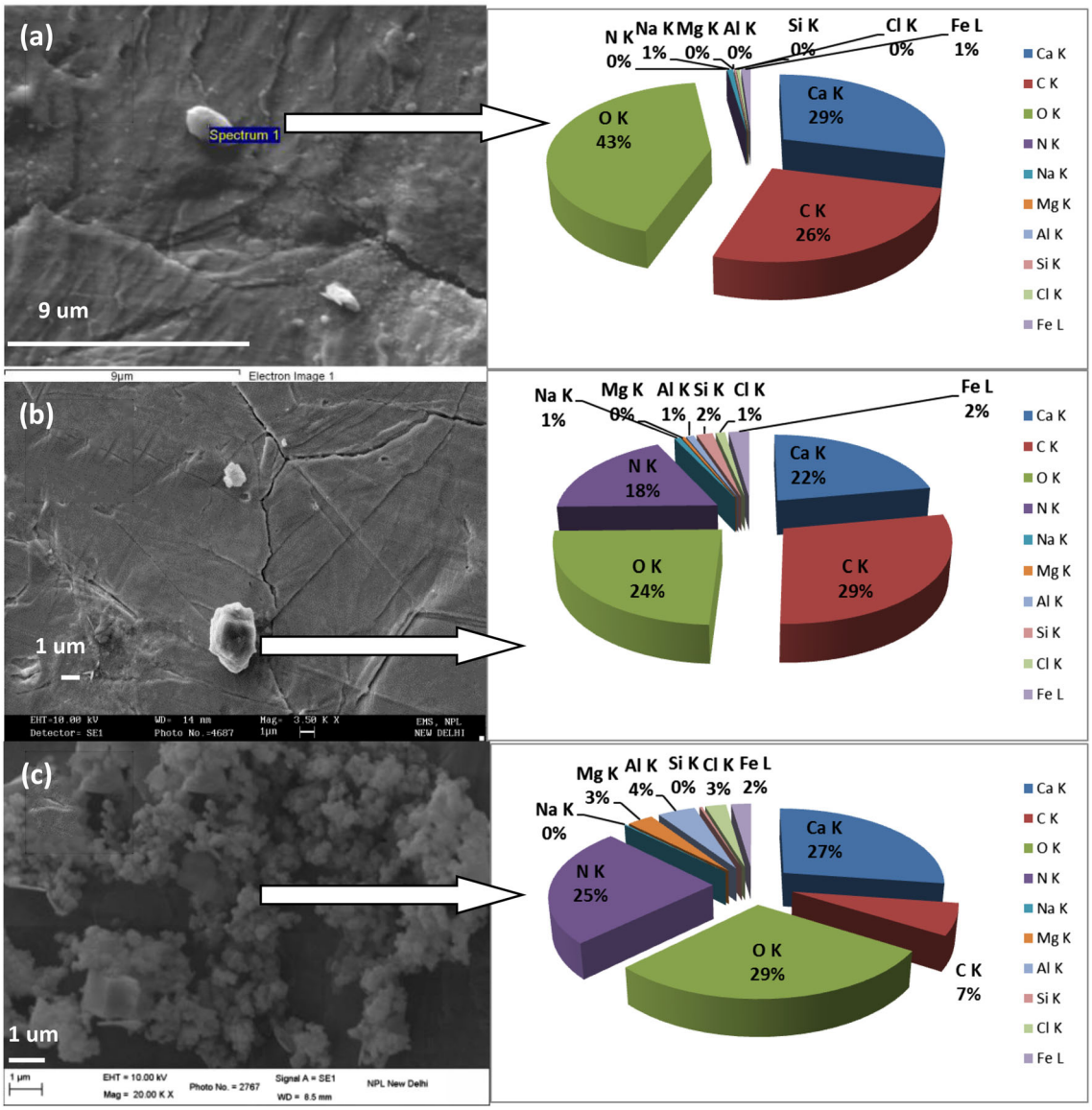


**Fig. 5** Morphology, composition, and mixing state of individual calcite particles based on SEM-EDS analysis

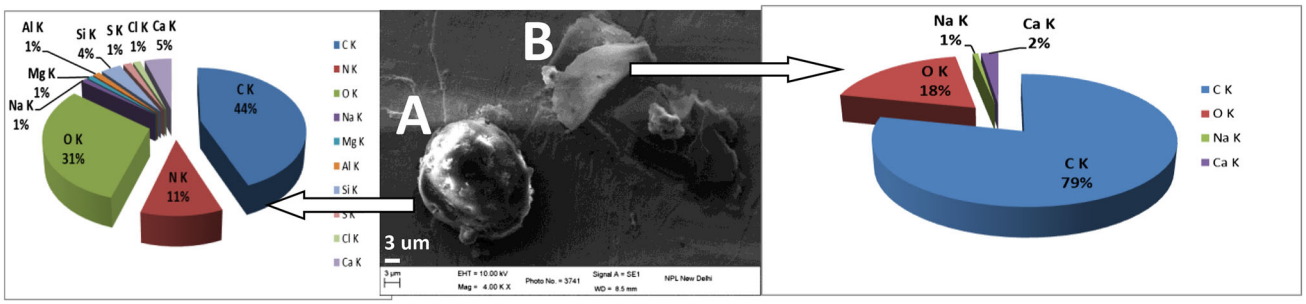


**Fig. 6** Morphology and composition of individual biological particles based on SEM-EDS analysis

flakes rich in Fe, Cr, B, C and S. Particles rich in Fe (>40%) were found in Fig. 7d and (i) with abundance of S and also traces of C, Si, K, Mg and Al. Figure 7d shows the flakes rich in Fe (45%). Presence of this excessive Fe in atmosphere may be due to some anthropogenic activities. We also found Ti (∼25%) rich particle in Fig. 7e.

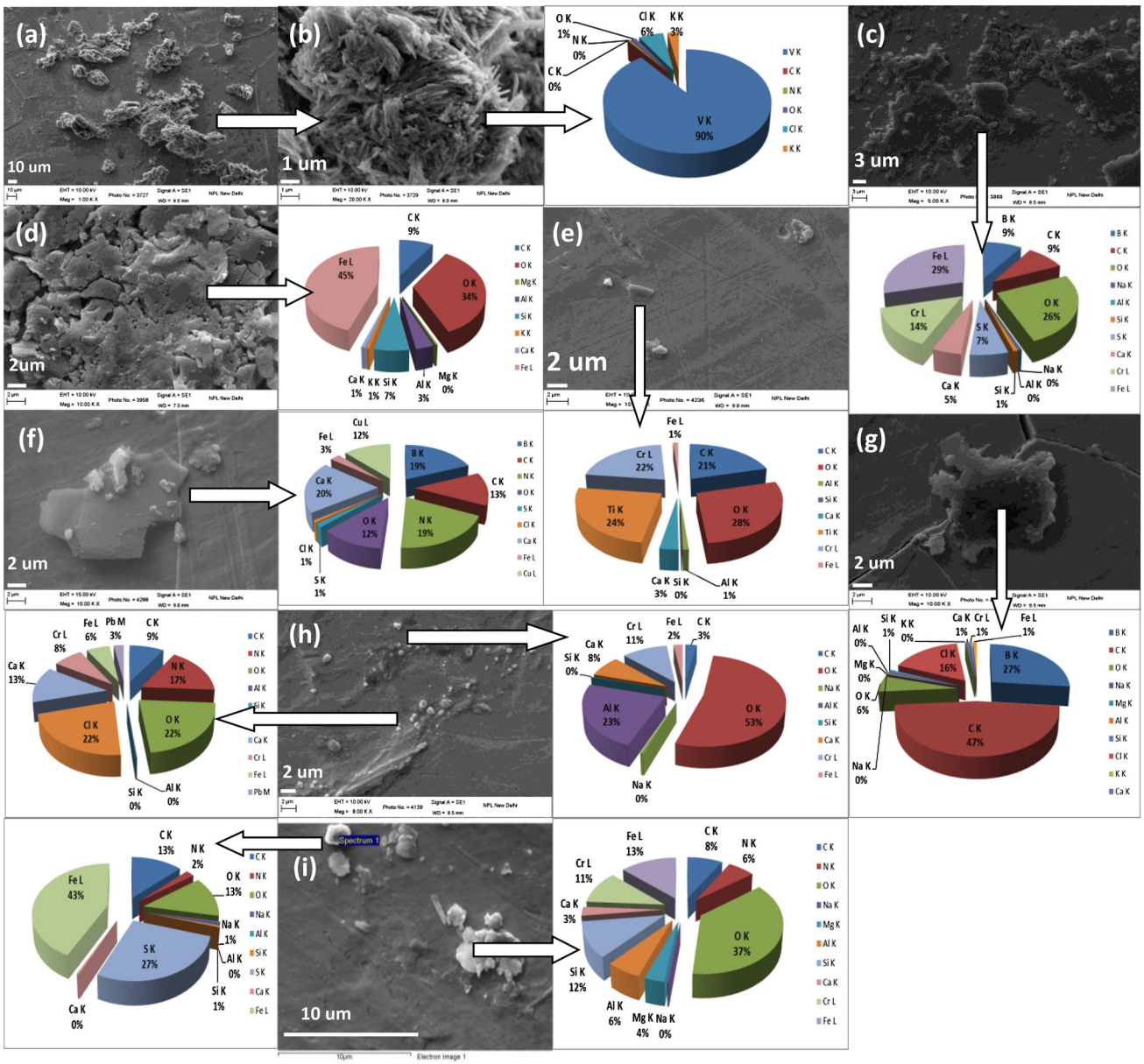


**Fig. 7** Morphology and composition of individual anthropogenic particles and their complex mixture with dust based on SEM-EDS analysis

The oxides of Cr ($Cr_2O_3$ and $CrO_3$) have anthropogenic origin from industries as these oxides are used in electroplating and processing of ferrous and non-ferrous alloys. Airborne particles at this site are found to be rich in metals as shown in Fig. 7. The particles were observed with Cr, ≥10 and >20% in Fig. 7c, h, i and e, respectively while C, Fe, N and Si were found in traces. Figure 7e shows a flake mainly composed of Ti, Cr and C. Figure 7g shows the flaky particle rich in C (∼47%), Cl (∼16%) and B (∼27%) with traces of Fe and Si. Figure 7f shows a flake of coarse size with 19% concentration of B; the emission of B in the atmosphere is due to some anthropogenic activity. Figure 7h shows the sub-micron size mineral dust spheres which were found to be mixed with Cl, Cr, and Pb. Figure 7i shows the spheroidal shape particle (left) mainly composed of FeS and aged with C while the other particle (right) was found to be mineral dust mixed with Cr.

## 4.2. Variation in Fe and Hematite ($Fe_2O_3$) Percentage

As discussed earlier, hematite in aerosol plays an important role in the absorption of solar radiation hence the quantification of the same is essential. Figure 8 shows the proportions (number wt%) of particles with varying Fe wt% range. 61% particles were observed with 0–2% Fe wt% range while 5% of particles represent Fe >20 wt%.

**Table 1** The number percentage of particles with varying Fe wt% range

| S. no. | Proportion of particles (number %) | Fe (wt% range) | $Fe_2O_3$ (wt% range) | $Fe_2O_3$ (volume% range) |
|---|---|---|---|---|
| 1 | 61 | 0 to ≤2 | 0 to ≤2.86 | 0 to ≤1.43 |
| 2 | 7 | >2 to ≤4 | >2.86 to ≤5.71 | >1.43 to ≤2.86 |
| 3 | 7 | >4 to ≤6 | >5.71 to ≤8.57 | >2.86 to ≤4.29 |
| 4 | 8 | >6 to ≤8 | >8.57 to ≤11.43 | >4.29 to ≤5.72 |
| 5 | 2 | >8 to ≤10 | >11.43 to ≤14.29 | >5.72 to ≤7.12 |
| 6 | 0 | >10 to ≤12 | >14.29 to ≤17.15 | >7.12 to ≤8.58 |
| 7 | 10 | >12 to ≤20 | >17.15 to ≤28.59 | >8.58 to ≤14.30 |
| 8 | 5 | >20 | >28.59 | >14.30 |

Hematite ($Fe_2O_3$) weight and volume percentage range have also been shown for given elemental Fe wt%

Table 1 shows the number percentage of particles with varying Fe elemental weight percentage range. Following the approach by Agnihotri et al. [12], hematite ($Fe_2O_3$) weight and volume percentage ranges have also been calculated and shown in the Table 1. Based on AERONET retrievals, Koven and Fung [58] inferred the range of hematite volume fraction for the global mineral dust to be 3.75–11.97%. Formenti et al. [59] observed that the hematite contribution from the dust vary largely. Based on a study in Jaipur, near Thar Desert, India (semi-arid zone) during winter 2012, Agnihotri et al. [12] reported hematite volume percentage in aerosols in the range 1.10–5.68%. In the present study, the hematite contribution of<14 volume % may be due to mineral dust while >14% may be due to anthropogenic activities.

### 4.3. Morphological Parameter (AR) of Regional Particles

AR is the morphological parameter that indicates the extent of particle non-sphericity. The SEM images of individual PM10 particles, collected during different months, were recorded and then used for calculation of morphological factors using Image-J software following the approach by Mishra et al. [4]. Figure 9 shows the frequency distribution of AR of sampled particles during different months. The numbers of individual particles considered for the analysis for every month have also been shown in the brackets in the respective months. PM10 with AR range between >1.2 to ≤1.4 was found to be dominant throughout the entire studied period except during June when majority of the particles are characterized with AR in the range range >1.4 to ≤1.6. This may be due to dust storm conditions which enhanced the occurrence of more non-spherical particles over the sampling site. During this month, we also observed the enhancement of particles with high AR (>2 to ≤2.2). The dust storm over South-Western Asia was observed by MODIS satellite on June 1, 2011 (http://earthobservatory.nasa.gov/NaturalHazards/view.php?id=50781). The dust plumes arising from the Middle East blew from the source towards South-East Asia. The particles which are spherical and close to spherical shape (AR range 1.0 to ≤1.2) were found to be less than 20% throughout the experiment with the least percentage (11.5%) during June. In general, the AR frequency distributions show the bimodal distribution (except for April month) with two mode peaks for AR ranges >1.2 to ≤1.4 and >1.8 to ≤2.0; however, the mode peaks were found to be shifted for the particles collected during June. Table 2 shows the classification of the sampled particles based on the range of AR. Particles with spherical shape or close to spherical shape (AR: 1.0 to ≤1.2) are denoted as "Sph"; particles with moderate non-spherical shape (AR: >1.2 to ≤1.6) denoted as "Nsp-1"; particles with further increased non-sphericity (AR: >1.6 to ≤2) denoted as "Nsp-2"; highly non-spherical shape (AR: >2 to ≤2.8) denoted as "Nsp-3";and extreme non-sphericity are denoted as "Nsp-4". The proportions of the particles lying in the aforesaid categories during various months have also been shown in number percentage. This AR proportion data is very important for modelers to reduce the uncertainty associated with the numerical estimation of optical and radiative properties of the regional particles over Kanpur in the IGP. The application of HESA will lead to significant uncertainty in the forcing estimation. Therefore, we have refrained from HESA application over the study region.

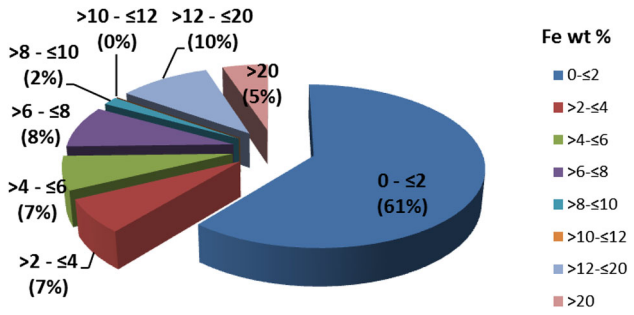


**Fig. 8** Proportions of particles (shown in *brackets*) with Fe wt% range based on SEM-EDS analysis of all the particles

**Table 2** Classification of particle non-sphericity based on AR range and their proportions in number percentage for study period, April–July, 2011

| S. no. | Classification of particle non-sphericity | Nomenclature | AR range | Proportions (number %) | | | |
|---|---|---|---|---|---|---|---|
| | | | | April, 2011 | May, 2011 | June, 2011 | July, 2011 |
| 1 | Sphere + Smooth shape | Sph | 1.0 to ≤1.2 | 14.8 | 19.3 | 11.5 | 14.7 |
| 2 | Moderate non-spherical | Nsp-1 | >1.2 to ≤1.6 | 42.4 | 41.0 | 43.1 | 39.9 |
| 3 | Non-spherical | Nsp-2 | >1.6 to ≤2 | 22.4 | 18.0 | 22.4 | 23.9 |
| 4 | Highly non-spherical | Nsp-3 | >2 to ≤2.8 | 14.3 | 13.0 | 16.7 | 13.5 |
| 5 | Extreme non-spherical | Nsp-4 | >2.8 | 6.2 | 8.7 | 6.3 | 8.0 |

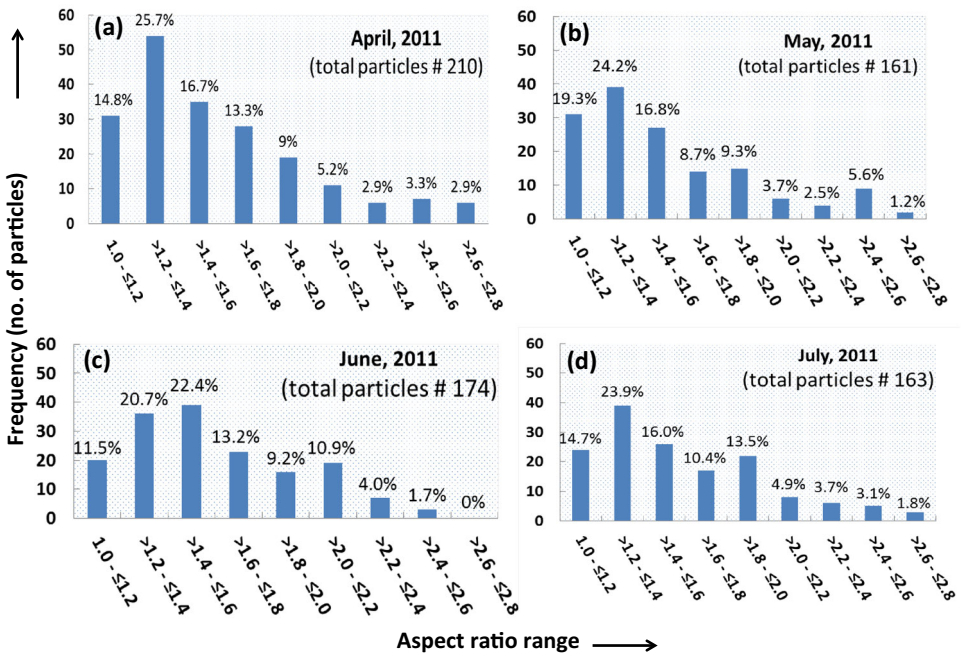


**Fig. 9** Frequency distribution of aspect ratio range for particles collected during **a** April, **b** May, **c** June and **d** July, 2011

## 5. Conclusions

Over IGP, a region where long range transported mineral dust form a complex mixture with local pollution, the data on composition, morphology and mixing state of individual particles is extremely important. Till date, there is no detailed observation of the said properties over Kanpur in IGP. To fill this gap, a field campaign was carried out at Kanpur (IITK; 26.52°N, 80.23°E, 142 m msl), India from April to July, 2011. The individual particle analyses reveal four classes of major particles: (a) Cu rich particles mixed with carbon and sulphur (b) dust and clays mixed with carbonaceous species (c) Fe rich particles mixed with carbon and sulfur and (d) Calcite ($CaCO_3$) particles aged with Nitrate. Carbonaceous particles were observed in various morphologies. The spot EDS analysis of 67 particles reveal that 61% particles have Fe weight percentage in the range 0 to ≤2%, while 5% particles have Fe >20 wt%. The frequency distributions of AR of total 708 particles from April to June reveal that particles with AR range >1.2 to ≤1.4 were abundant throughout the experiment except during June when it was found to shift to high AR range of >1.4 to ≤1.6 (followed with another peak of AR from >2 to ≤2.4) due to dust storm conditions enhancing the occurrence of more non-spherical particle over the sampling site. The spherical particles (and close to spherical shape; AR range 1.0 to ≤1.2) were found to be less than 20% throughout the experiment with a minimum (11.5%) during June.

The individual particle analyses of aerosol morphology, composition and mixing performed in the present study reveals that the routine HESA assumption in the optical and radiative model is not relevant and may lead to erroneous forcing estimations. The use of representative AR and hematite content (observed during the campaign) in the radiative model will improve the radiative forcing estimation over the region. However; in future, statistically significant, size segregated frequency distributions of AR,

hematite content, proportions of mixing states data is required to further refine the regional radiative forcing and improve the retrievals of regional aerosol properties.

**Acknowledgements** Authors are thankful to Director NPL for his consistent support for the ongoing work. Authors acknowledge CSIR Network Project AIM_IGPHim (PSC-0112) and ISRO-GBP for the financial support.

## References

[1] IPCC, The physical science basis. Contribution of working group I to the fourth assessment report of the intergovernmental panel on climate change, vol 825; Cambridge University Press, Cambridge (2007).

[2] IPCC, Climate change 2013: the physical science basis. Contribution of working group I to the fifth assessment report of the intergovernmental panel on climate change; Cambridge University Press, Cambridge, (2013).

[3] P.R. Buseck and M. Pósfai, Airborne minerals and related aerosol particles: effects on climate and the environment. Proc. Natl. Acad. Sci., **96** (1999) 3372-3379.

[4] S.K. Mishra, R. Agnihotri, P.K. Yadav, S. Singh, M.V.S.N. Prasad, P.S. Praveen, J.S. Tawale, Rashmi, N.D. Mishra, B.C. Arya and C. Sharma, Morphology of atmospheric particles over semi-arid region (Jaipur, Rajasthan) of India: implications for optical properties. Aerosol Air Qual. Res., (2015). doi: 10.4209/aaqr.2014.10.0244.

[5] S.G. Aggarwal, Recent developments in aerosol measurement techniques and the metrological issues. MAPAN-J. Metrol. Soc. India, **25** (2010) 165-189.

[6] S.G. Aggarwal, S. Kumar, P. Mandal, B. Sarangi, K. Singh, J. Pokhariyal, S.K. Mishra, S. Agarwal, D. Sinha, S. Singh, C. Sharma and P.K. Gupta, Traceability issue in PM2.5 and PM10 measurements. MAPAN-J. Metrol. Soc. India, **28** (2013) 153-166. doi:10.1007/s12647-013-0073-x.

[7] A. Awasthi, B.-S. Wu, C.-N. Liu, C.-W. Chen, S.-N. Uang and C.-J. Tsai, The effect of nanoparticle morphology on the measurement accuracy of mobility particle sizers. MAPAN-J. Metrol. Soc. India, **28** (2013) 205-215. doi:10.1007/s12647-013-0068-7.

[8] H. Volten, O. Munoz, J.W. Hovenier, J.F. de Hann, W. Vassen, et al., WWW scattering matrix database for small mineral particles at 441.6 and 632.8 nm. J. Quant. Spectrosc. Radiat. Transf., **90** (2005) 191-206.

[9] S.K. Mishra and S.N. Tripathi, Modeling optical properties of mineral dust over the Indian Desert. J. Geophys. Res., **113** (2008) D23201. doi:10.1029/2008JD010048.

[10] S.K. Mishra, S. Tripathi, S.G. Aggarwal and A. Arola, Optical properties of accumulation mode, polluted mineral dust: effects of particle shape, hematite content and semi-external mixing with carbonaceous species. Tellus Ser. B, **64** (2012) 19-25.

[11] I.N. Sokolik and O.B. Toon, Incorporation of mineralogical composition into models of the radiative properties of mineral aerosol from UV to IR wavelengths. J. Geophys. Res., **104** (1999) 9423-9444.

[12] R. Agnihotri, S.K. Mishra, P. Yadav, S. Singh, Rashmi, M.V.S.N. Prasad, B.C. Arya and C. Sharma, Bulk level to individual particle level chemical composition of atmospheric dust aerosols (PM5) over a semi-arid zone of western India (Rajasthan). Aerosol Air Qual. Res., **15** (2015) 58-71.

[13] J.E. Post and P.R. Buseck, Characterization of individual particles in the Phoenix Urban aerosol, using electron beam instruments. Environ. Sci. Technol., **18** (1984) 35-42.

[14] M. Pósfai and P.R. Buseck, Nature and climatic effects of individual tropospheric aerosol particles. Annu. Rev. Earth Planet. Sci., **38** (2010) 17-43.

[15] S. Tiwari, A.S. Pipal, P.K. Hopke, D.S. Bisht, A.K. Srivastava, S. Tiwari, P.N. Saxena, A.H. Khan, S. Pervez, Study of the carbonaceous aerosol and morphological analysis of fine particles along with their mixing state in Delhi, India: a case study. Environ. Sci. Pollut. Res. Int., (2015) 10744-10757. doi: 10.1007/s11356-015-4272-6.

[16] Z. Cong, S. Kang, S. Dong, X. Liu and D. Qin, Elemental and individual particle analysis of atmospheric aerosols from high Himalayas. Environ. Monit. Assess., **160** (2010) 323-335.

[17] W. Li, L.Y. Shao, R. Shen, Z. Wang, S. Yang and U. Tang, Size, composition and mixing stateof individual aerosol particles in South China Coastal City. J. Environ. Sci. **22** (2010) 561-569.

[18] V. Murari, M. Kumar, N. Singh, R.S. Singh and T. Banerjee, Particulate morphology and elemental characteristics: variability at middle Indo-Gangetic Plain. J. Atmos. Chem., **73** (2016) 165-179. doi:10.1007/s10874-015-9321-5.

[19] T. Pachauri, V. Singla, A. Satsangi, A. Lakhani, K.M. Kumari, SEM-EDX characterization of individual coarse particles in Agra, India. Aerosol. Air Qual. Res., **13** (2013) 523-536. doi: 10.4209/aaqr.2012.04.0095.

[20] A.S. Pipal, R. Jan, P.G. Satsangi, S. Tiwari, A. Taneja, Study of surface morphology, elemental composition and origin of atmospheric aerosols ($PM_{2.5}$ and $PM_{10}$) over Agra, India. Aerosol Air Qual. Res., **14** (2014) 1685-1700. doi: 10.4209/aaqr.2014.01.0017.

[21] N. Chinnam, S. Dey, S.N. Tripathi and M. Sharma, Dust events in Kanpur, northern India: chemical evidence for source and implications to radiative forcing. Geophys. Res. Lett., **33** (2006) L08803. doi:10.1029/2005GL025278.

[22] S. Ghosh, T. Gupta, N. Rastogi, A. Gaur, A. Misra, S.N. Tripathi, D. Paul, V. Tare, O. Prakash, D. Bhattu, A.K. Dwivedi, D.S. Kaul, R. Dalai and S.K. Mishra, Chemical characterization of summertime dust events at Kanpur: insight into the sources and level of mixing with anthropogenic emissions. Aerosol Air Qual. Res., **14** (2014) 879-891.

[23] A. Misra, A. Gaur, D. Bhattu, S. Ghosh, A.K. Dwivedi, R. Dalai, D. Paul, T. Gupta, S.K. Mishra, S. Singh, S.N. Tripathi and V. Tare, An overview of the physico-chemical characteristics of dust at Kanpur in the central Indo-Gangetic basin. Atmos. Environ., **97** (2014) 386-397.

[24] O.V. Kalashnikova and I.N. Sokolik, Modeling the radiative properties of nonspherical soil-derived mineral aerosols. J. Quant. Spectrosc. Radiat. Transfer., **87** (2004) 137-166.

[25] K. Okada, J. Heintzenberg, K. Kai and Y. Qin, Shape of atmospheric mineral particles collected in three Chinese arid-regions. Geophys. Res. Lett., **28** (2001) 3123-3126.

[26] J. Li, J.R. Anderson and P.R. Buseck, TEM study of aerosol particles from clean and polluted marine boundary layers over the North Atlantic., J. Geophys. Res., **108** (2003). doi: 10.1029/2002JD002106.

[27] J. Li, M. Pósfai, P. Hobbs and P.R. Buseck, Individual aerosol particles from biomass burning in southern Africa: compositions and aging of inorganic particles. J. Geophys. Res., **108** (2003). doi:10.1029/2002JD002310.

[28] M. Pósfai, R. Simonics, J. Li, P.V. Hobbs and P.R. Buseck, Individual aerosol particles from biomass burning in sourthern Africa: 1. Compositions and size distributions of carbonaceous particles. J. Geophys. Res., **108** (2003). doi: 10.1029/2002JD002291.

[29] H. Yuan, K.A. Rahn and G. Zhuang, Graphical techniques for interpreting the composition of individual aerosol particles. Atmos. Environ. **38** (2004) 6845-6854.

[30] M. Pósfai, A. Gelencser, R. Simonics, K. Arato, J. Li, P.V. Hobbs and P.R. Buseck, Atmospheric tar balls: Particles from biomass and biofuel burning. J. Geophys. Res., **109** (2004) D06213. doi:10.1029/2003JD004169.

[31] C. Johansson, M. Norman and L. Burman, Road traffic emission factors for heavy metals. Atmos. Environ., **43** (2009) 4681-4688.

[32] H.A. Schroeder, M. Dobson and D.M. Kane, Toxic trace elements associated with airborne particulate matter: a review. J. Air Pollut. Control Assoc., **37** (1987) 1267-1285.

[33] WHO Report, Air quality guidelines for Europe, 2nd Ed, WHO Regional Publications, European Series, No. 91, ISBN 92 890 1358 3, ISSN 0378-2255 (2000).

[34] D.J. Greenland, J.M. Oades and T.W. Sherwin, Electron microscope observations of iron oxides in some red soils. J. Soil Sci., **19** (1968) 123-126.

[35] K. Kandler, N. Benker, U. Bundke, E. Cuevas, M. Ebert, P. Knippertz, S. Rodriguez, L. Schütz and S. Weinbruch, Chemical composition and complex refractive index of Saharan mineral dust at Izana, Tenerife (Spain) derived by electron microscopy. Atmos. Environ., **41** (2007) 8058-8074.

[36] K. Kandler, L. Schütz, C. Deutscher, M. Ebert, H. Hofmann, S. Jäckel, R. Jaenicke, P. Knippertz, K. Lieke, A. Massling, A. Petzold, A. Schladitz, B. Weinzierl, A. Wiedensohler, S. Zorn and S. Weinbruch, Size distribution, mass concentration, chemical and mineralogical composition and derived optical parameters of the boundary layer aerosol at Tinfou, Morocco, during SAMUM 2006, Tellus B **61** (2009) 32-50. doi: 10.1111/j.1600-0889.2008.00385.x.

[37] S. Lafon, J. Rajot, S. Alfaro and A. Gaudichet, Quantification of iron oxides in desert aerosol. Atmos. Environ., **38** (2004) 1211-1218.

[38] E.A. Reid, J.S. Reid, M.M. Meier, M.R. Dunlap, S.S. Cliff, A. Broumas, K. Perry and H. Maring, Characterization of African dust transported to Puerto Rico by individual particle and size segregated bulk analysis. J. Geophys. Res., **108** (2003). doi: 10.1029/2002jd002935.

[39] A. Petzold, A. Veira, S. Mund, M. Esselborn, C. Kiemle, B. Weinzierl, T. Hamburger, G. Ehret, K. Lieke and K. Kandler, Mixing of mineral dust with urban pollution aerosol over Dakar (Senegal): impact on dust physico-chemical and radiative properties. Tellus B., **63** (2011) 619-634.

[40] A.D. Clarke, Y. Shinozuka, V.N. Kapustin, S. Howell and B. Huebert, Size distributions and mixtures of dust and black carbon aerosol in Asian outflow: physiochemistry and optical properties. J. Geophys. Res., **109** (2004). doi:10.1029/2003JD004378.

[41] S. China, C. Mazzoleni, K. Gorkowski, A.C. Aiken and M.K. Dubey, Morphology and mixing state of individual freshly emitted wildfire carbonaceous particles. Nat. Commun., **4** (2013) 2122. doi:10.1038/ncomms3122.

[42] O. Popovicheva, E. Kireeva, N. Persiantseva, T. Khokhlova, N. Shonija, V. Tishkova and B. Demirdjian. Effect of soot on immersion freezing of water and possible atmospheric implications. Atmos. Res. **90** (2008) 326-337.

[43] R. Zhang, A.F. Khalizov, J. Pagels, D. Zhang, H. Xue and P.H. McMurry, Variability in morphology, hygroscopicity, and optical properties of soot aerosols during atmospheric processing. Proc. Natl. Acad. Sci., **105** (2008) 10291-10296.

[44] D. Trochkine, Y. Iwasaka, A. Matsuki, M. Yamada and Y.S. Kim, Mineral aerosol particles collected in Dunhuang, China, and their comparison with chemically modified particles collected over Japan. J. Geophys. Res. Atmos., **108** (2003). doi: 10.1029/2002jd003268.

[45] D.Z. Zhang, J.Y. Zang, G.Y. Shi, Y. Iwasaka, A. Matsuki, et al., Mixture state of individual Asian dust particles at a coastal site of Qingdao, China. Atmos. Environ. **37** (2003) 3895-3901.

[46] A. Matsuki, A. Schwarzenboeck, H. Venzac, P. Laj, S. Crumeyrolle and L. Gomes, Cloud processing of mineral dust: direct comparison of cloud residual and clear sky particles during AMMA aircraft campaign in summer 2006. Atmos. Chem. Phys., **10** (2010) 1057-1069.

[47] B.J. Krueger, V.H. Grassian, A. Laskin and J.P. Cowin, The transformation of solid atmospheric particles into liquid droplets through heterogeneous chemistry: laboratory insights into the processing of calcium containing mineral dust aerosol in the troposphere. Geophys. Res. Lett., **30** (2003). doi: 10.1029/2002GL016563.

[48] B.J. Krueger, V.H. Grassian, J.P. Cowin and A. Laskin, Heterogeneous chemistry of individual mineral dust particles from different dust source regions: the importance of particle mineralogy. Atmos. Environ., **38** (2004) 6253-6261.

[49] A. Laskin, M.J. Iedema, A. Ichkovich, E.R. Graber, I. Taraniuk and Y. Rudich, Direct observation of completely processed calcium carbonate dust particles. Faraday Discuss., **130** (2005) 453-468.

[50] A. Matsuki, Y. Iwasaka, G.Y. Shi, D.Z. Zhang, D. Trochkine, M. Yamada, Y.S. Kim, B. Chen, T. Nagatani, T. Miyazawa, M. Nagatani and H. Nakata, Morphological and chemical modification of mineral dust: observational insight into the heterogeneous uptake of acidic gases. Geophys. Res. Lett., **32** (2005) L22806. doi:10.1029/2005GL024176.

[51] J.T. Kelly and A.S. Wexler, Thermodynamics of carbonates and hydrates related to heterogeneous reactions involving mineral aerosol. J. Geophys. Res., **110** (2005) D11201. doi: 10.1029/2004JD005583.

[52] S. Matthias-Maser and R. Jaenicke, Examination of atmospheric bioaerosol particles with radii $> 0.2$ mm. J. Aerosol Sci., **25** (1994) 1605-1613.

[53] S. Matthias-Maser, V. Obolkin, T. Khodzer and R. Jaenicke, Seasonal variation of primary biological aerosol particles in the remote continental region of Lake Baikal/Siberia. Atmos. Environ., **34** (2000) 3805-3811.

[54] X. Chen, P. Ran, K. Ho, W. Lu, B. Li, Z. Gu, C. Song and J. Wang, Concentrations and size distributions of airborne microorganisms in Guangzhou during summer. Aerosol Air Qual. Res., **12** (2012) 1336-1344.

[55] E. Coz, B. Artíñano, L.M. Clark, M. Hernandez, A.L. Robinson, G.S. Casuccio, T.L. Lersch and S.N. Pandis, Characterization of fine primary biogenic organic aerosol in an Urban Area in the Northeastern United States. Atmos. Environ., **44** (2010) 3952-3962.

[56] L. Deguillaume, M. Leriche, P. Amato, P.A. Ariya, A.M. Delort, U. Pöschl, N. Chaumerliac, H. Bauer, A.I. Flossmann and C.E. Morris, Microbiology and atmospheric processes: chemical interactions of primary biological aerosols. Biogeoscience **5** (2008) 1073-1084.

[57] B.C. Deotare, M.D. Kajale, S.N. Rajaguru, S. Kusumgar, A.J.T. Jull and J.D. Donahue Paleoenvironmental history of Bap-Malar and Kanod playas of western Rajasthan Thar Desert. Proc. Indian Acad. Sci. **113** (2004) 403-425.

[58] C.D. Koven and I. Fung, Inferring dust composition from wavelength-dependent absorption in Aerosol Robotic Network (AERONET) data. J. Geophys. Res., **111** (2006) D14205. doi: 10.1029/2005JD006678.

[59] P. Formenti, L. Schuetz, Y. Balkanski, K. Desboeufs, M. Ebert, K. Kandler, A. Petzold, D. Scheuvens, S. Weinbruch, D. Zhang, Recent progress in understanding physical and chemical properties of African and Asian mineral dust. Atmos. Chem. Phys., **11** (2011) 8231–8256.